REPORT DOCUMENTATION PAGE

Form Approved
OMB No. 0704-0188

1. REPORT DATE *(DD-MM-YYYY)*	2. REPORT TYPE	3. DATES COVERED *(From - To)*
13-07-2007	Final Technical Report	Feb. 1, 2004 - Jan. 31, 2007

4. TITLE AND SUBTITLE
Quantum Lattice Algorithms for Nonlinear Physics: Optical Solutions and Bose-Einstein Condensation

5a. CONTRACT NUMBER

5b. GRANT NUMBER
FA9550-04-1-0044

5c. PROGRAM ELEMENT NUMBER

6. AUTHOR(S)
George Vahala
gvahala@gmail.com

5d. PROJECT NUMBER

5e. TASK NUMBER

5f. WORK UNIT NUMBER

7. PERFORMING ORGANIZATION NAME(S) AND ADDRESS(ES)
The College of William and Mary
P.O. Box 8795
Williamsburg, VA 23187-8795

8. PERFORMING ORGANIZATION REPORT NUMBER

9. SPONSORING/MONITORING AGENCY NAME(S) AND ADDRESS(ES)
USAF, AFRL
AF OFFICE OF SCIENTIFIC RESEARCH
875 RANDOLPH STREET, SUITE 325, ROOM 3112
ARLINGTON, VA 22203-1768
Dr Jon A. Sjogren/NE

AFRL-SR-AR-TR-07-0272

12. DISTRIBUTION/AVAILABILITY STATEMENT
Distribution Statement A: unlimited

13. SUPPLEMENTARY NOTES

14. ABSTRACT
on separate sheet

15. SUBJECT TERMS

16. SECURITY CLASSIFICATION OF:			17. LIMITATION OF ABSTRACT	18. NUMBER OF PAGES	19a. NAME OF RESPONSIBLE PERSON
a. REPORT	b. ABSTRACT	c. THIS PAGE		10	Mark Roberts
					19b. TELEPHONE NUMBER *(include area code)* 757-221-3970

Using CAP resources we have been able to uncover lattice geometry effects in the entropic lattice Boltzmann algorithm that had not been expected from lower grid resolution runs. In the entropic formulation, one is working with a generalized BGK collision operator that has within it the germs of detailed balance. Thus, the unconditionally stable algorithm is achieved with a variable transport coefficient, not unlike Large Eddy Simulations (LES) in CFD. Indeed, we have explored this connection in some detail but will report those findings elsewhere due to space limitations here. Another unexpected result unearthed by the CAP runs was the dependence of the ELB on the Mach number. A low Mach number expansion has to be performed to analytically evaluate the Lagrange multipliers arising in the extremization of the H-function subject to local collisional constraints. We have found that the Qi 5-bit model is less sensitive to the flow Mach number than the Q27-bit model. Another somewhat unexpected finding was the importance of maintaining the distribution function correlations in the mesoscopic description. To perform the long-time 1 6OO~ grid runs we needed to perform continuation runs. In the early stages of CAP we tried to minimize the amount of i/o read-out/read-in and to reconstruct the relaxation distribution function from its moments rather than keeping the full correlation information. While this did not affect the energy decay, there were significant discontinuities introduced into the enstrophy and higher energy spectral moments.

The parallelization strength of ELB arises from the modeling of the macroscopic nonlinear derivatives by local moments. Chapman-Enskog asymptotics will then, on projecting back into physical space, yield these nonlinear derivatives. Indeed, this will allow ideally parallelized Smagorinsky type LES to be modeled by LB methods and in LB-MHD algorithms enforce automatically $\nabla \cdot B = 0$ without the recourse to expensive divergence cleaning algorithms.

The interconnection between quantum algorithms that can run on quantum (and classical) computers and ELB (that can only run on classical computers) has been outlined as well as a new morphology of free shear turbulence and the onset of laminar-to-turbulence transition. The analogy between

Order-disorder phase transition (Lattice) Ising Model

laminar-turbulence fluid transition Entropic Lattice Boltzmaim Model will be being strongly pursued in future proposals.

AFOSR FINAL REPORT

"DEVELOPMENT OF ALGORITHMS For NONLINEAR PHYSICS on TYPE-II QUANTUM COMPUTERS"

July 2007

George Vahala
William & Mary

During the 3 years of this grant, we have continued our collaboration with Jeffrey Yepez (AFRL, Hancom Field) and Linda Vahala (ODU) on both quantum and entropic lattice

algorithms for the solution of nonlinear physics problems. Because of the extreme scalability of the algorithms that we have been developing, we were chosen for CAP-Phase I for the new IBM-P5+ supercomputer (Babbage) at NAVO MSRC. Using the full 2912 processors available, we achieved 6.3 TFlops/s sustained performance – an excellent performance seeing that the maximum sustained Flop-rate is just over 20 TFlops/s. The scaling achieved by our entropic codes is near perfect for these algorithms - as seen by the Figure below.

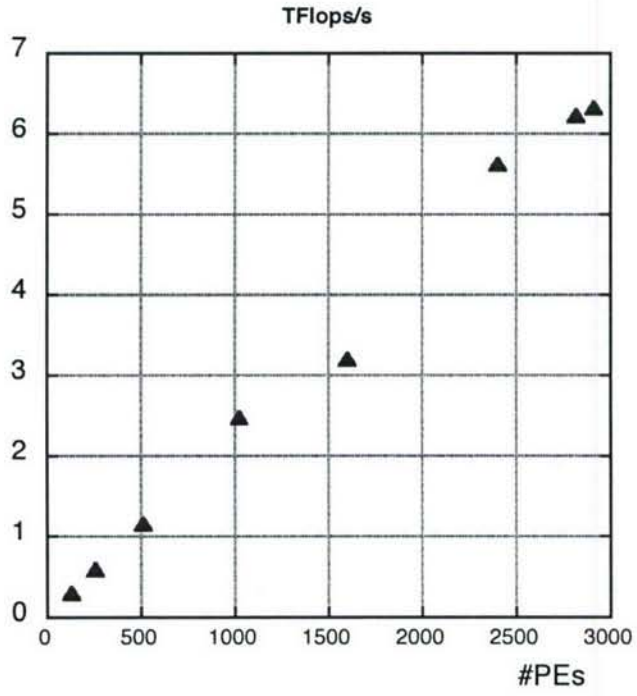

As a result, we were chosen to participate in CAP-Phase II and presented these results at the DoD-UGC 2007 meeting in Pittsburgh.

What is very interesting is the analogy between the detailed balance quantum lattice algorithms and entropic lattice Boltzmann algorithms.

At each space-time grid point $(\mathbf{x},t)$ in lattice algorithms, the excited state of a qubit $|q\rangle$ encodes the probability f_q of the existence of a mesoparticle moving with discrete lattice velocity $\mathbf{c}_q = \Delta\mathbf{x}_q / \Delta t$. $\Delta\mathbf{x}_q$ are the lattice vector links, with $q = 1,2, \ldots. Q$, where Q is the number of qubits at each spatial node. The particle momentum is determined from a suitably chosen qubit-qubit interaction Hamiltonian H' while the spatial location arises from the free-streaming Hamiltonian $-i\hbar\sum_q \mathbf{c}_q \cdot \nabla$. All the particle-particle interactions generated by H' (from 2-body up to Q-body interactions) can be mapped onto a local collision operator $\Omega_q\left(f_1 \ldots . f_Q\right)$ at $\mathbf{x}$. In particular, for type-II quantum algorithms, the

quantum entanglement is localized to those Q-qubits at $(\mathbf{x},t)$ and then this entanglement is spread throughout the lattice by unitary streaming[3,4]:

$$f_q'(\mathbf{x},t) = f_q(\mathbf{x},t) + \Omega_q(f_1....f_Q) \ , \ f_q(\mathbf{x}+\Delta\mathbf{x}_q, t+\Delta t) = f_q'(\mathbf{x},t) \quad . \tag{1}$$

Here f_q is the incoming probability and f_q' the outgoing probability. In the classical limit, there exists a fundamental discrete entropy function[1,2,5]

$$\mathrm{H}(f_1...f_Q) = \sum_{q=1}^{Q} f_q \ln(f_q / w_q), \tag{2}$$

where the normalized weights $\left(\sum_q w_q = 1\right)$ are determined self-consistently. The collision operator Ω_q in Eq. (1) is determined so that one remains on a constant entropy surface

$$\mathrm{H}(f_1'....f_Q') = \mathrm{H}(f_1...f_Q) \quad . \tag{3}$$

Eqs. (1)-(3) constitute the basics of the detailed-balance lattice algorithms for fluid turbulence that are ideal for parallel (both classical and quantum) supercomputers.

In the Q-dimensional velocity space, the relaxation distribution function f_q^{eq} is determined analytically by extremizing the H-function subject to the local collisional constraints of conservation of probability and probability flux. f_q^{eq}, considered as a vector, is the bisector of the difference between the incoming and outgoing kinetic vectors in the inviscid limit $\lim_{\mu\to 0} \alpha / 2\tau = 2$:

$$f_q = f_q^{eq} - \frac{2\tau}{\alpha}\Omega_q \ , \ f_q' = f_q^{eq} + \left(1 - \frac{2\tau}{\alpha}\right)\Omega_q \tag{4}$$

Eliminating Ω_q and f_q' from Eqs. (4) and (1) one obtains the lattice Boltzmann (LB) equation

$$f_q(\mathbf{x}+\Delta\mathbf{x}_q, t+\Delta t) = f_q(\mathbf{x},t) + \frac{\alpha}{2\tau}\left[f_q^{eq}(\mathbf{x},t) - f_q(\mathbf{x},t)\right] \ , \ q = 1....Q \tag{5}$$

This is basically the entropic LB[1,2] with the BGK collisional relaxation parameters $\alpha(\mathbf{x},t)/2\tau$ and f_q^{eq} determined from Eqs. (2) and (3). In the Chapman-Enksog limit, $(\Delta\mathbf{x}\to 0 \ , \ \Delta t \to 0)$-- and identifying the density and momentum moments $\sum_q f_q = \rho$, $\sum_q \mathbf{c}_q f_q = \rho\ \mathbf{u}$ -- one recovers the quasi-incompressible Navier-Stokes equation with

$$\text{effective viscosity: } \mu(\mathbf{x},t) = \frac{1}{6}\left(\frac{4\tau}{\alpha(\mathbf{x},t)} - 1\right) \ ;$$

$$\text{molecular viscosity: } \mu_0 = \frac{1}{6}(2\tau - 1) \ , \ \tau > 0.5 \tag{6}$$

To avoid discrete lattice geometry effects polluting the turbulence simulations, one is restricted to certain Q's on a cubic lattice. In particular it can be shown that on a unit cubic lattice, the lowest order kinetic velocity models are

Q15: rest velocity, speed 1 (6 velocities), speed $\sqrt{3}$ (8 velocities) – i.e., $Q = 15$

Q19: rest velocity, speed 1 (6 velocities), speed $\sqrt{2}$ (12 velocities) – i.e., $Q = 19$

Q27: rest velocity, speed 1 (6), speed $\sqrt{2}$ (12), and speed $\sqrt{3}$ (8) – i.e., $Q = 27$ (7)

Because detailed balance is in-built into the entropic LB algorithm [see Eq. (3)], the scheme is unconditionally stable for arbitrary large Reynolds numbers, $\mathrm{Re} = U_0 L / 2\pi\mu_0$.

In Table below we show the wallclock time and average performance of the various ELB models for the full 2912 PEs available for 2000 LB time steps. The Q27 model, based on the 27 kinetic streaming vectors, is the most memory intensive (about 1 KB/grid point) and requires a wallclock time which is over 1.5 times that required by the Q15 model (which requires just 0.5 KB/grid point).

#PEs	GRID	MODEL	WALLCLOCK (s)	GFlops/s per PE
2912	ca1950^3	ELB-Q27	7 554.7	2.17
2912	ca1950^3	ELB-Q19	5 602.7	2.24
2912	ca1950^3	ELB-Q15	4 798.4	2.05

Table 1 : *GFlops/s per CPU for 2912 CPUs for 2000 time steps for the 3 ELB-codes.*

For CAP-Phase II we wished to investigate the role of the underlying kinetic lattice symmetry on Navier-Stokes turbulence, since all three ELB-algorithms recover the Navier-Stokes equations to leading order in the Chapman-Enskog expansion. This is particularly important since on small grids (e.g., 512^3) and low molecular viscosities ($\mu_0 = 2 \times 10^{-4}$) we[4] had found very minor differences in the simulation results from the Q27, Q19 and Q15 models. With 2048 PEs available for 24 hour shifts, the maximal spatial grid for the Q27 algorithm was 1600^3. All 3 models were run with the same base parameters : $u_0 = 0.035$, $\mu_0 = 5 \times 10^{-4}$ on the 1600^3-grid (i.e., with a base $\mathrm{Re} = u_0 L / 2\pi\mu_0 \approx 18{,}000$ and computational resolution/grid spacing $\mathrm{Re}^{3/4} / L \approx 1$) for a Kida initial velocity profile[6] with delta-function energy spectra.

In Fig. 2 we plot the normalized kinetic energy $< \left|\mathbf{u}(\mathbf{x},t)\right|^2 > / < \left|\mathbf{u}(\mathbf{x},0)\right|^2 >$, the normalized enstrophy $< \left|\boldsymbol{\omega}(\mathbf{x},t)\right|^2 > / < \left|\boldsymbol{\omega}(\mathbf{x},0)\right|^2 >$, the palinstrophy 2 $P(t)$ = $< \left|\nabla \times \boldsymbol{\omega}\right|^2 >$, where the vorticity $\boldsymbol{\omega} = \nabla \times \mathbf{u}$, and < .. > represent volume average over the periodic domain. The ELB-dissipation rate $\varepsilon(t)$ is defined by $\varepsilon(t) = 2\mu_{eff}(t) \left\langle S_{ij} S_{ij} \right\rangle$, where S_{ij} is the usual rate of strain tensor and the effective relaxation rate (to make an analogy with standard LB algorithms)

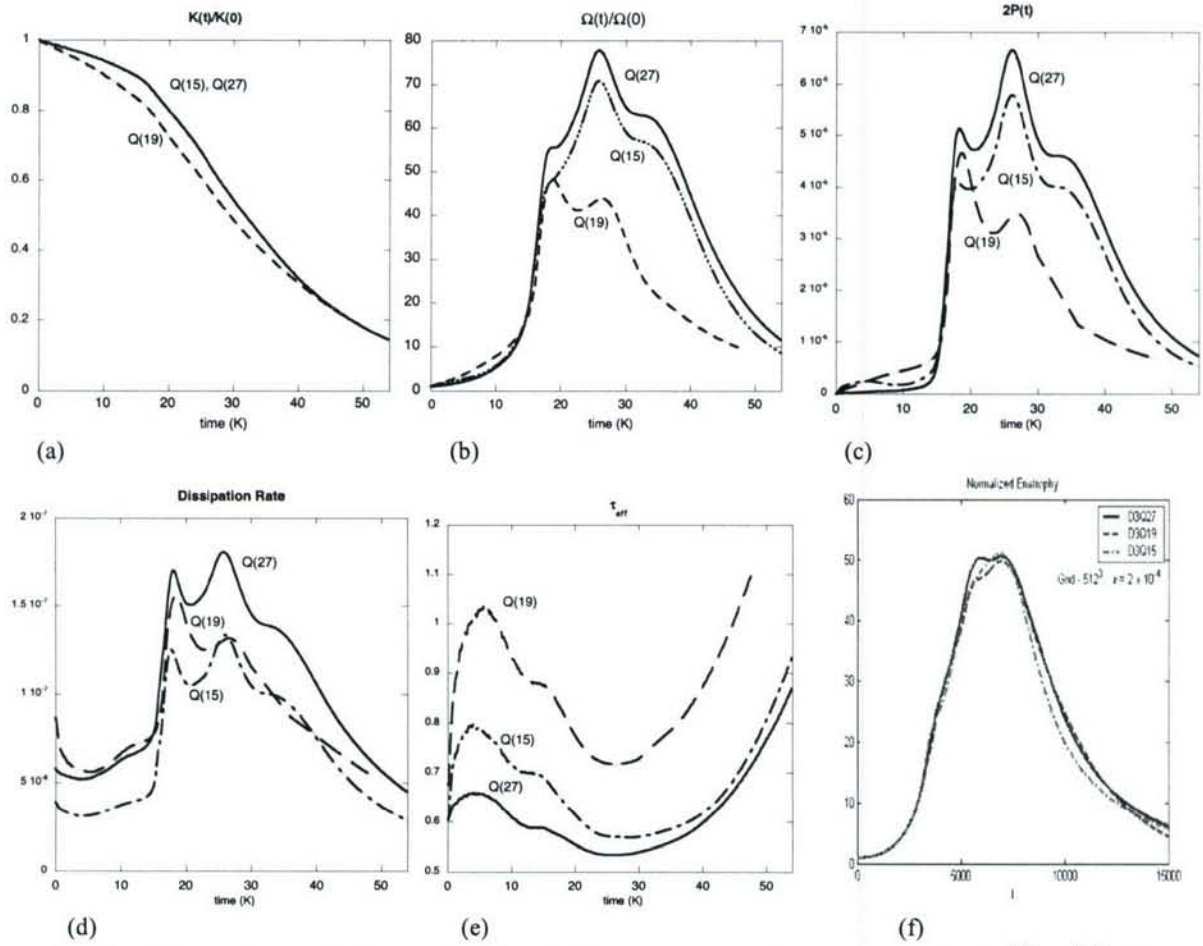

Fig. 2 *The evolution of the normalized (a) kinetic energy K(t)/K(0), (b) enstrophy* $\Omega(t)/\Omega(0)$ *,(c) palinstrophy P(t) (d) dissipation rate* $\varepsilon(t)$*, (e)* τ_{eff} *for the Q27, Q19 and Q15 algorithms on* 1600^3*-grid with (f) normalized enstrophy from a* 512^3*-simulation at somewhat lower molecular viscosity.*

$\mu_{eff}(t) = \left(<4\tau/\alpha(\mathbf{x},t)> - 1\right)/6$. Clearly the Q19-results significantly deviates even qualitatively from the Q27- and Q15-results, while there is strong quantitative agreement between the Q27- and Q15- models (up to a simple rescaling). This contrasts strongly with a low-resolution grid run on 512^3 at a somewhat lower molecular viscosity, see Fig. 2(f). It appears that these differences arise from the Newton-Raphson root finder that determines at each grid point and at each time the $\alpha(\mathbf{x},t)$ function that enforces detailed balance on the constant entropic surface, Eq. (3). These functions $\alpha(\mathbf{x},t)$ seem to be much more lattice-dependent, i.e., whether Q27, Q19 or Q15, than would have been gleaned from small grid runs.

In Fig. 3 we plot the development of the longitudinal and transverse 1D energy spectra :

$$E_{long}(k_x,t) = \sum_{k_y,k_z} \left|v_x(\mathbf{k},t)\right|^2 \quad , \quad E_{trans}(k_x,t) = \sum_{k_y,k_z} \left|v_y(\mathbf{k},t)\right|^2 \tag{8}$$

for the initial Kida velocity profile[6] with initial delta function spectra

$$E_{long}(k_x,0) = E_0\delta(k_x-2) \quad , \text{ and } \quad E_{trans}(k_x,0) = E_1\left[\delta(k_x-2)+\delta(k_x-4)\right] \tag{9}$$

While the terabytes of data from the early stages (t < 28 K) of the Q27-run are being retrieved and analyzed, some of the data from the t ≥ 28 K has been analyzed. The energy spectra approximately obey a $k^{-5/3}$ Kolmogorov law, with a slight upturn at the very large k_x in E_{long}, indicating that the run is slightly unresolved at these scales

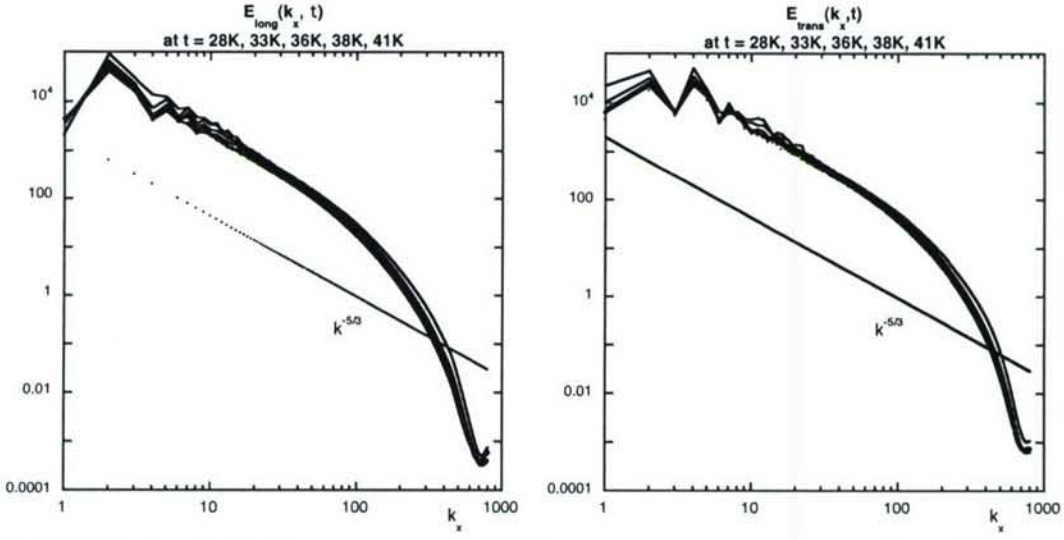

Fig. 3(a) *The longitudinal energy spectrum, (b) the transverse energy spectrum for t > 28 K.*

The probability distribution functions (pdfs) for the velocity and vorticity components are shown in Fig. 4. The velocity field is basically Gaussian – but with tails that are substantially higher than a Guassian. These tails die out with time as seen by the plot of $P\left[v_x\right]$ at t = 29K (Fig. 4a) and at t = 41K (Fig. 4b). The pdfs for the other velocity components have very similar behavior. On the other hand, the vorticity pdf is well fitted by an exponential pdf. This is indicative of intermittency in the turbulence:

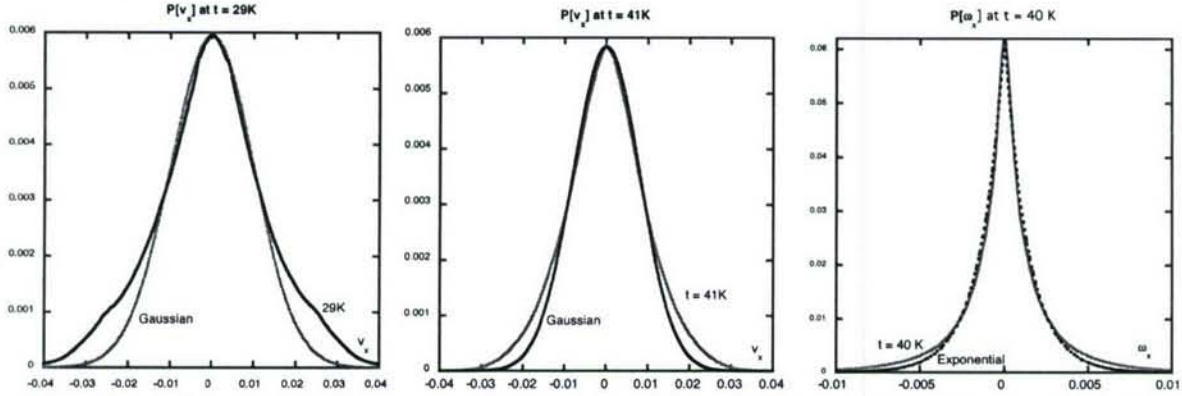

Fig. 4 *The pdf for the velocity component v_x at (a) t = 29K, and (b) t = 41K, fitted to Gaussian pdfs. The pdf for the vorticity component ω_x at t = 40K is shown in (c), fitted to an exponential pdf.*

Turbulence Morphology for Free Shear Turbulence

We have started to examine a somewhat new turbulence morphology of free shear turbulence and the correlation between the onset of turbulence in a laminar-to-turbulence transition and the order-disorder phase transition in ferromagnetism. Just as Ising lattice models are fundamental to understanding critical phenomena, kinetic lattice gas models that we are pursuing could have a similar impact. We now give some preliminary results on the turbulence morphology from 512^3 grid runs. The morphology can be broken down into 3 main stages, Fig. 5. Stage 1 occurs in the initial time interval $0 < t < 3.2K$ with the enstrophy $\Omega(t)$ increases exponentially, independent of the viscosity. The enstrophy curve is plotted in Fig. 5 with the integer dots '1'. '2' ... '7' – and these integers correspond to the isosurfaces of constant vorticity at t = 1K, t = 2K ... t = 7K in Fig. 5. The color coding is based on the value of $\hat{\mathbf{u}} \cdot \hat{\boldsymbol{\omega}}$: grey corresponds to $\hat{\mathbf{u}} \cdot \hat{\boldsymbol{\omega}} =$ -, blue for $\hat{\mathbf{u}} \cdot \hat{\boldsymbol{\omega}} = +1$ and red for $\hat{\mathbf{u}} \cdot \hat{\boldsymbol{\omega}} = -1$. In this initial stage, the isosurfaces of vorticity are stretched with a sharp rise in $d\Omega / dt$ (the sharply rising curve above the enstrophy curve in Stage 1). In Stage 2, for time $3.2K < t < 9K$, shown shaded in Fig. 5, there is large scale anisotropic turbulence with intermittency. In this shaded region $d\Omega / dt$ becomes jagged and predominantly is decreasing in large spurts with intermediate avalanches occurring at t = 5.1K, and 6.75K (vertical red lines in Stage 2 of Fig. 5). Stage 3, for $9K < t < 14K$, is the inertial subrange with eventual exponential decay of the enstrophy (see curve fitted red line that fits $\Omega(t)$ well for t > 10K). In this Stage 3, we see the onset of homogeneous isotropic small scale turbulence with energy cascading to small scales leading to the Kolmogorov $k^{-5/3}$ energy spectrum. The velocity pdf is Gaussian while the vorticity pdf is exponential (see the inset plots in Fig. 5).

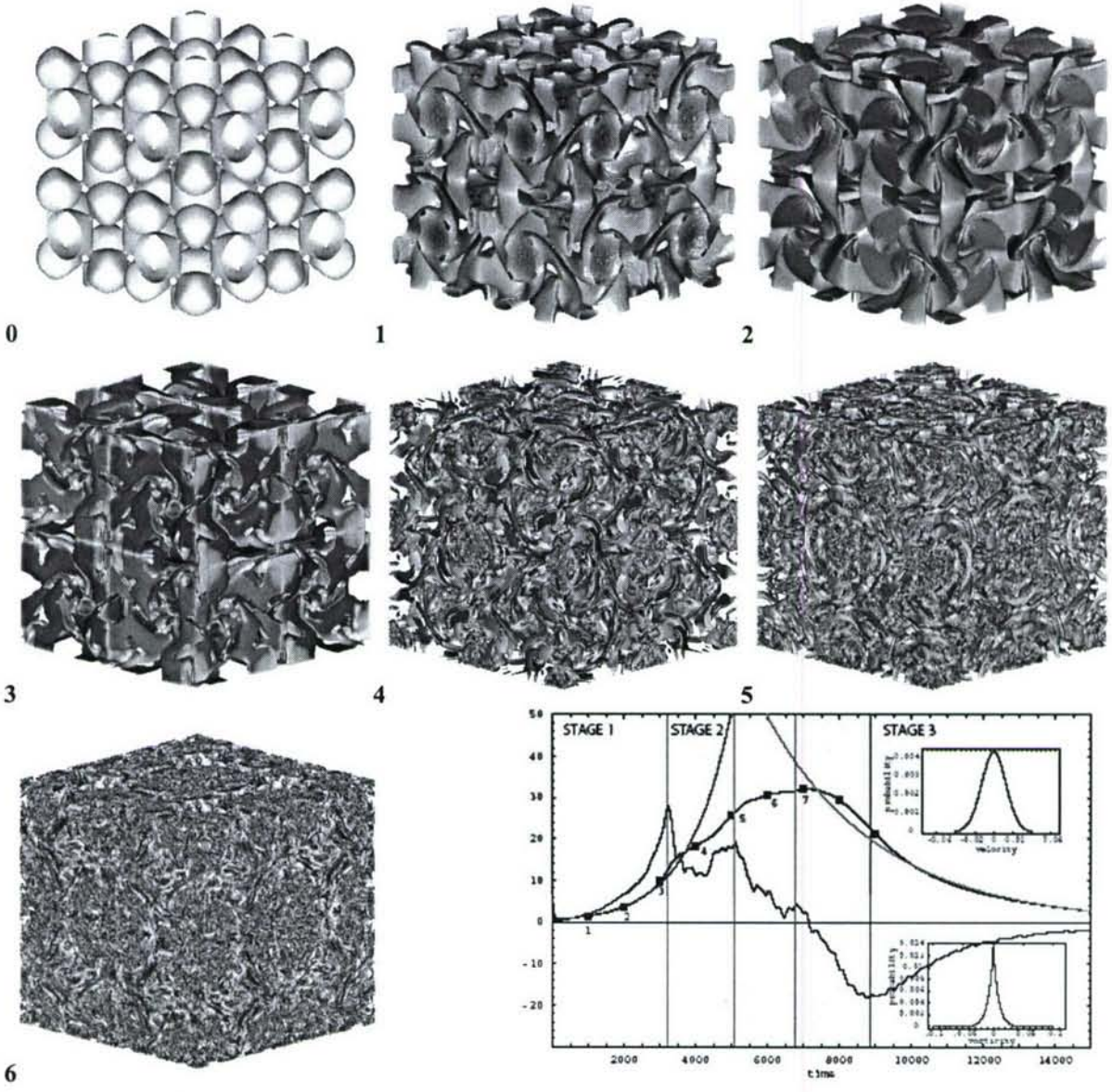

Fig. 5 *Surfaces of constant vorticity from t = 0K to t = 7K, color coded by* $\hat{\mathbf{u}} \cdot \hat{\boldsymbol{\omega}}$ *[grey = 0, blue = +1, red = -1].* ***Stage 1: 0 < t < 3.2K.*** *Vortex stretching, with an exponential growth in the enstrophy* $\Omega(t)$ *- the 1....7 corresponds to vorticity isosurface plots.* ***Stage 2: 3.2K < t < 9K.*** *Large scale anisotropic turbulence and intermittency occur. The major breaking points are at 3.2K, 5.1K and 6.8K (red lines in enstrophy plot).* ***Stage 3: t > 9K.*** *inertial subrange with homogeneous isotropic small scale turbulence with* $k^{-5/3}$ *Kolmogorov energy*

Concluding Remarks

Using CAP resources we have been able to uncover lattice geometry effects in the entropic lattice Boltzmann algorithm that had not been expected from lower grid resolution runs. In the entropic formulation, one is working with a generalized BGK collision operator that has within it the germs of detailed balance. Thus, the unconditionally stable algorithm is achieved with a variable transport coefficient, not unlike Large Eddy Simulations (LES) in CFD. Indeed, we have explored this connection in some detail but will report those findings elsewhere due to space limitations here. Another unexpected result unearthed by the CAP runs was the dependence of the ELB on the Mach number. A low Mach number expansion has to be performed to analytically evaluate the Lagrange multipliers arising in the extremization of the H-function subject to local collisional constraints. We have found that the Q15-bit model is less sensitive to the flow Mach number than the Q27-bit model. Another somewhat unexpected finding was the importance of maintaining the distribution function correlations in the mesoscopic description. To perform the long-time 1600^3 grid runs we needed to perform continuation runs. In the early stages of CAP we tried to minimize the amount of i/o read-out/read-in and to reconstruct the relaxation distribution function from its moments rather than keeping the full correlation information. While this did not affect the energy decay, there were significant discontinuities introduced into the enstrophy and higher energy spectral moments.

The parallelization strength of ELB arises from the modeling of the macroscopic nonlinear derivatives by local moments. Chapman-Enskog asymptotics will then, on projecting back into physical space, yield these nonlinear derivatives. Indeed, this will allow ideally parallelized Smagorinsky type LES to be modeled by LB methods and in LB-MHD algorithms enforce automatically $\nabla \cdot \mathbf{B} = 0$ without the recourse to expensive divergence cleaning algorithms.

The interconnection between quantum algorithms that can run on quantum (and classical) computers and ELB (that can only run on classical computers) has been outlined as well as a new morphology of free shear turbulence and the onset of laminar-to-turbulence transition. The analogy between

Order-disorder phase transition $\leftrightarrow$ (Lattice) Ising Model
laminar-turbulence fluid transition $\Leftrightarrow$ Entropic Lattice Boltzmann Model

will be being strongly pursued in future proposals.

Publications During this Grant Proposal

"Entropic Lattice Boltzmann Representations Required to Recover Navier-Stokes Flows"
B. Keating, G. Vahala, J. Yepez, M. Soe and L. Vahala
Physical Review **E75**, 036712 [1-11] (2007)

"Lattice Model of Fluid Turbulence"
J. Yepez, G. Vahala, L. Vahala, M. Soe and S. Ziegeler
Navigator NAVO MSRC , Spring 2007, pp. 12-19

"Lattice Boltzmann Algorithms for Fluid Turbulence"
G. Vahala, J. Yepez, M. Soe, L. Vahala and S. Ziegeler
IEEE Proc. Comp. Sci. (submitted), 2007

"Quantum Lattice Representations for Vector Solitons in External Potentials"
G. Vahala, L. Vahala and J. Yepez
Physica **A362**, 215-221 (2006)

"Performance of Lattice Boltzmann Codes for NAvier-Stokes and MHD Turbulence on the Major Computer Architectures"
G. Vahala, J. Carter, M. Soe, J. Yepez, L. Vahala and A. Macnab
Parallel CFD 2005 (Elseiver Press, 2006)

"Lattice Quantum Algorithm for the Schrodinger Wave Equation in 2+1 Dimensions with a Demonstration by Modeling Soliton Instabilities"
J. Yepez, G. Vahala and L. Vahala
Quantum Info. Process. **4**, 457- 469 (Dec. 2005)

"Quantum Lattice Representation of 1D MHD turbulence with arbitrary Transport Coefficients"
J. Yepez, G. Vahala and L. Vahala
SPIE Conf. Proc. **5815**, 227-235 (2005)

"Magnetohydrodynamic Turbulence Simulations on the Earth Simulator Using the Lattice Boltzmann Method"
J. Carter, M. Soe, L. Oliker, Y. Tsuda, G. Vahala, L. Vahala and A. Macnab
International Conf. on High Computing, SC|05 (Nov. 2005, Seattle), Gordon-Bell Finalist Paper ISBN #1-59593-061-2

"Inelastic Vector Soliton Collisions: A Quantum Lattice Gas Representation"
G. Vahala, L. Vahala and J. Yepez
Phil. Trans.. Roy Soc. London **362**, 1677 – 1690 (2004)

"Quantum lattice gas representation of dark solitons"
G. Vahala, L. Vahala, and J. Yepez
SPIE Conf. Proc. **5436**, 376 – 385 (2004)